Park et al. *NPG Asia Materials* (2018) 10: 959–969
DOI 10.1038/s41427-018-0080-z

NPG Asia Materials

ARTICLE Open Access

Fully laser-patterned stretchable microsupercapacitors integrated with soft electronic circuit components

Sangbaek Park[1], Hyub Lee[2], Young-Jin Kim[2] and Pooi See Lee[1]

Abstract

Stretchable energy storage devices are prerequisites for the realization of autonomous elastomeric electronics. Microsupercapacitors (MSCs) are promising candidates for this purpose due to their high power and energy densities, potential for miniaturization, and feasibility of embedding in circuits; however, efforts to realize stretchable MSCs have mostly relied on strain-accommodating materials and have suffered from limited stretchability, low conductivity, or complicated patterning processes. Here, we designed and fabricated a stretchable MSC based on reduced-graphene-oxide/Au heterostructures patterned by facile and versatile direct laser patterning. An interconnected and stable 3D network composed of vertically oriented heterostructures was realized by high-repetition-rate femtosecond laser pulses. Upon transferring to polydimethylsiloxane (PDMS), the 3D network achieved a high conductivity of ~10^5 S m^{-1}, and the conductivity could be maintained at ~10^4 S m^{-1} even at 50% strain. A fully laser-patterned stretchable electronics system was integrated with embedded MSCs, which will find applications in soft robotics, wearable electronics, and the Internet of Things.

Introduction

Stretchable energy storage devices that can accommodate large strain while retaining their electrochemical functions are the key components of power elastomeric electronics to make them truly autonomous systems[1–5]. Microsupercapacitors (MSCs) are promising candidates because they can be easily miniaturized on chips as discrete power sources[6]. Additionally, their in-plane structure is beneficial to realize an ultrahigh power density and a high-frequency response[7]. The fabrication of MSCs is enabled by patterning or printing technologies that are simple, scalable, and cost-effective and can provide versatile designs, functions, and aesthetics[8–11]. While some flexible MSCs have been demonstrated using laser writing[12,13], inkjet printing[14–16], or screen printing[17], these approaches have rarely been adopted in stretchable MSCs because the electrode materials used cannot accommodate large strain due to their stiff mechanical properties and interfacial adhesion issues or mechanical incompatibility with the elastomeric substrates.

Fully soft electronics contain materials and components that need to be mechanically robust and stretchable; for example, molecularly stretchable electronics, stretchable transistors, and stretchable in-plane batteries have been attempted[18–21]. Recently, Bao's group reported stretchable organic transistors using intrinsically stretchable semiconductors that maintained 67 and 19% of their original mobility at 20% and 50% strain, respectively[20]. These intrinsically stretchable transistors endured a stretching durability test at 25% strain and 500 cycles. Wang's group also reported an intrinsically stretchable Zn-Ag_2O in-plane battery using polystyrene-block-polyisoprene-block-polystyrene (SIS) as an elastic binder, where the resistance of the current collector increased

Correspondence: Young-Jin Kim (yj.kim@ntu.edu.sg) or Pooi See Lee (pslee@ntu.edu.sg)
[1]School of Materials Science and Engineering, Nanyang Technological University (NTU), 50 Nanyang Avenue, Singapore 639798, Singapore
[2]School of Mechanical and Aerospace Engineering, Nanyang Technological University (NTU), 50 Nanyang Avenue, Singapore 639798, Singapore
These authors contributed equally: Sangbaek Park and Hyub Lee

11.2 times at 100% strain[21]. However, an intrinsically fully stretchable MSC has not yet been achieved. Research has focused primarily on stretchable interconnections adopting serpentine circuits[22–24] or stretchable sealing/packing (such as a honeycomb PDMS substrate[25]) for MSC development; however, the MSCs themselves were not stretchable. For example, the honeycomb PDMS structure allowed the whole device to be stretched up to 150% without obvious performance decay because the maximum strain on the rigid MSCs was less than 3%, as stated in the report. Some previous researchers attempted to make stretchable MSCs by designing wavy-structured electrodes adhered to prestrained tripod-structured polydimethylsiloxane (PDMS)[26] or by injecting an electrode slurry into a wavy-shape-engraved PDMS mold[27]. However, these MSCs exhibited extrinsic stretchability that depended on the prestrained templates before material deposition, limiting their design and integration with other electronics[25]. Furthermore, all the MSCs described above were fabricated by complicated processes, such as photolithography, casting, or molding[7,27]. Therefore, a simple and versatile direct patterning method for producing intrinsically stretchable MSCs has been an urgent goal yet remained challenging to date.

Graphene offers great potential for energy storage due to its high theoretical surface area and electrical conductivity[13]. The in-plane architecture of an MSC can further increase the accessibility of a two-dimensional graphene electrode, as the edges of the electrodes are exposed to the electrolyte, allowing high power performance[7]. In addition, graphene has attracted considerable attention for use in stretchable electronic devices due to its extremely high mobility and good mechanical properties[28]. Laser patterning is a simple and flexible microfabrication technology that can be used to simultaneously reduce a graphene oxide (GO) film and scribe a reduced-graphene-oxide (rGO) pattern in designed geometries with micrometer resolution[12,13,29]. Such a technique can be realized with a consumer-grade LightScribe DVD burner, yielding a higher throughput than other methods[13]. However, MSCs directly fabricated from laser-treated GO on rigid or flexible substrates have been found to suffer from a lower rate capability compared to MSCs patterned using conventional photolithography with a rigid metal layer as a current collector[30,31]. This is because the resultant rGO was required to assume the role of an active material without the presence of metal current collectors[11–13,29]. This may give rise to more severe degradation in performance in an elastomeric system; for instance, the resistance of rGO was found to increase 14-fold when it was transferred to PDMS and by a factor of 100 when subjected to 50% tensile strain[32]. Hence, an innovative approach to improve both conductivity and stretchability of laser-scribed rGO electrodes is essential.

In this study, we propose laser-patterned vertical rGO/Au bilayer heterostructures for realizing intrinsically stretchable MSCs. Although metal nanoparticles (NPs)[33] or nanowires (NWs)[10] have been used to enhance the conductivity of patterned/printed rGO electrodes[34], the adhesion of rGO flakes is poor, and the rGO electrodes lose their electrical conductivity under high levels of stretching. Here, a vertically oriented rGO array fabricated by high-repetition-rate femtosecond laser pulse irradiation enables each rGO sheet to be covered with a thin Au layer and transferred to PDMS, as shown in the schematics in Fig. 1a. Our work offers a versatile and facile approach to prepare intrinsically stretchable porous structures for MSCs using a direct laser-patterning process and a direct transfer method, resulting from the differences in adhesion forces between the irradiated and unirradiated structures. Our approach has been used to successfully fabricate intrinsically stretchable MSCs without any prestrain process or complicated synthetic needs. The advantages of this intrinsically stretchable MSC are its multidirectional stretchability, space savings, and ability to be mounted on various substrates. The rGO/Au/PDMS exhibits high conductivity and stretchability, comparable to and compatible with recently reported intrinsically stretchable non-MSC-based devices[20,21]. This breakthrough can be attributed to two effects: one is the low junction resistance created by the heterostructure, and the other is the 3D connected network that reduces the contact loss even in a stretched state. Furthermore, laser patterning enables versatile designs; our intrinsically stretchable MSCs can be directly integrated in elastic electronic circuit components such as foldable switches, elastic resistors, and capacitors. Therefore, our intrinsically stretchable MSCs with arbitrarily patterned electrodes can be implemented in numerous applications, including interactive wearable devices, human-machine interfaces, smart robots, and the Internet of Things (IoT).

Materials and methods

Electrode and device fabrication

GO was prepared using a modified Hummer's method[35]. An aqueous dispersion of GO (2 mg mL^{-1}) was sonicated for 2 h and then drop-casted on a glass substrate with an area density of 0.21 mL cm^{-2} or 0.053 mL cm^{-2} (for irradiation with a 1030-nm or 515-nm wavelength laser) and allowed to dry overnight at room temperature. Vertically oriented rGO was obtained by direct laser writing with a Yb-doped fiber femtosecond laser (pulse duration, 220 fs). The laser wavelength, power, repetition rate, scan width, scan direction, and scanning

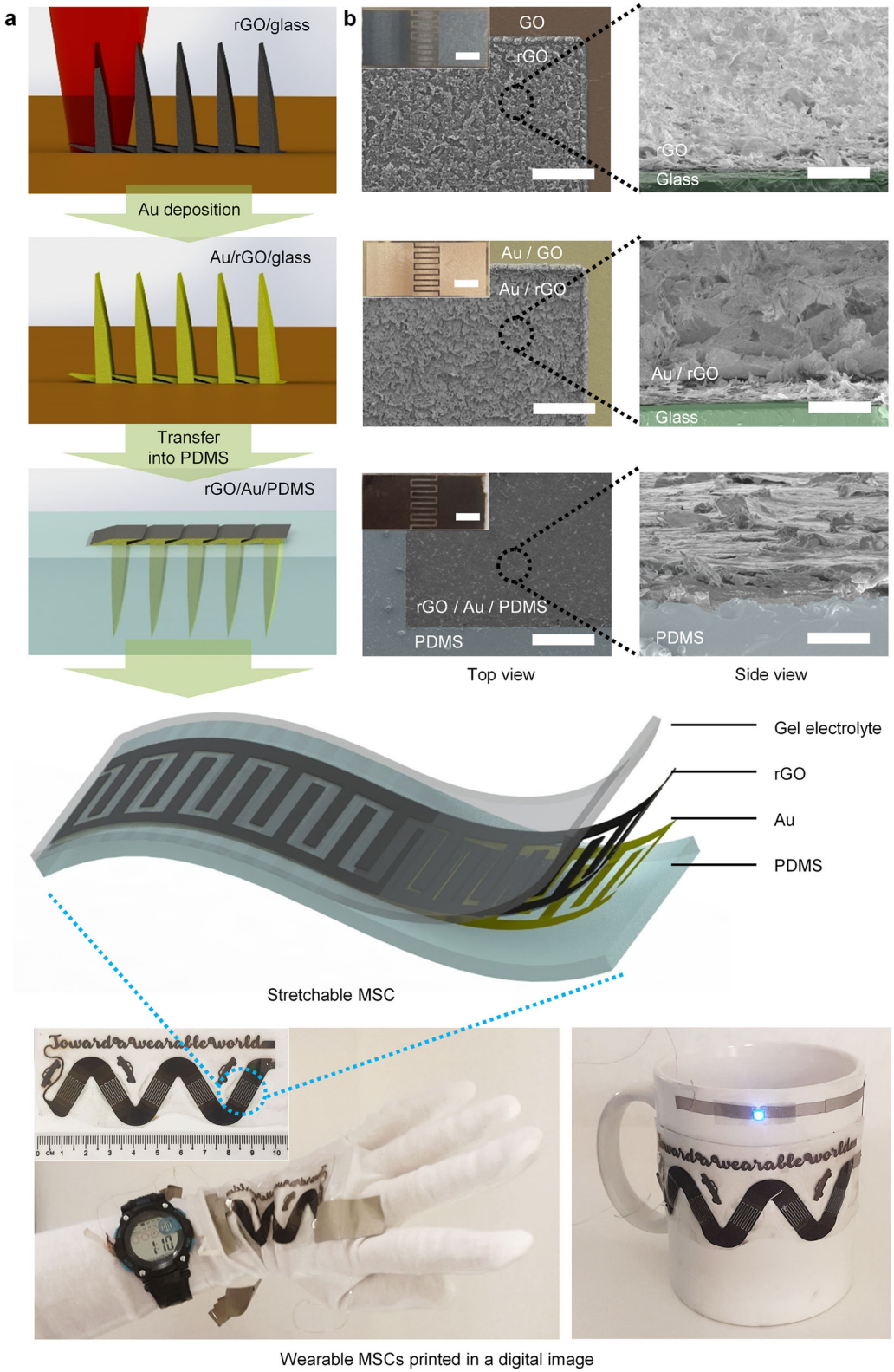

Fig. 1 (See legend on next page.)

(see figure on previous page)
Fig. 1 Design of the laser-patterned rGO/Au/PDMS microsupercapacitors and their application in deformable electronics. a Schematics of the fabrication process (from top to bottom): laser patterning of rGO on a glass substrate, deposition of an Au layer leading to the formation of rGO/Au heterostructures, transfer of rGO/Au to a PDMS elastomer, and assembly of rGO/Au/PDMS MSCs with a PVA/H_2SO_4 gel electrolyte. The photos show examples of MSCs printed in digital images and demonstrate their wearability by means of embedding on a long-sleeved glove or a mug and their use to power a digital watch or a blue LED. **b** Top-view (left) and tilted-view (right) scanning electron microscopy (SEM) images and photos (insets) corresponding to three fabrication schemes: rGO/glass, Au/rGO/glass, and rGO/Au/PDMS. Scale bars: 300 μm (top views), 30 μm (tilted views), and 5 mm (insets)

speed were modulated for a comparative study. Rectangular patterns and interdigitated micropatterns were designed for the laser writing of electrodes and MSCs, respectively. A layer of Au was deposited on the as-prepared rGO/glass by sputtering at a current of 20 mA for 0.2 h. Finally, a polydimethysiloxane (PDMS; Sylgard 184; Dow Corning) precursor was poured on the Au/rGO/glass. After being cured at 80 °C for 2.5 h, the elastomeric rGO/Au/PDMS film was carefully peeled off in deionized (DI) water.

Characterization and measurements

Materials characterizations were conducted by field emission scanning electron microscopy (JEOL 7600 F), optical microscopy, surface profilometry (KLA Tencor ASIQ), X-ray diffraction (Bruker D8 Advance), Raman spectroscopy (Witec alpha300 SR, 532 nm), and atomic force microscopy (Asylum Research Cypher S). The electrode conductivities (S, S m^{-1}) were calculated from the I–V curves measured using a Keithley Semiconductor Characterization System (4200-SCS) by equation 1:

$$S = \frac{l}{t \times w}\frac{1}{R} \tag{1}$$

where l, t, w, and R are the electrode length, thickness, width, and resistance, respectively. Cyclic voltammetry (CV), galvanostatic charge-discharge (GCD), and electrochemical impedance spectroscopy (EIS) were carried out using an Autolab PGSTAT30 potentiostat. An AC voltage with a 5-mV amplitude was applied in a frequency range of 0.01–100 kHz at open circuit voltage for EIS. The H_2SO_4/PVA gel was drop-cast on the active interdigitated electrode area as an electrolyte[31] and left at room temperature for 4 h to ensure that the electrolyte diffused into the electrode. An additional polyaniline (PANI) layer was electrodeposited on the rGO/Au/PDMS film in a solution of 0.03 M aniline and 1 M H_2SO_4 through CV (potential range, 0–1 V vs. Ag/AgCl; scan rate, 0.1 V s^{-1}).

Parameter calculation for the electrochemical performance of the MSCs

The specific areal capacitances (C_A, F cm^{-2}) were calculated from the CV curves and the GCD curves by equations 2 and 3:

$$C_{\mathrm{A}} = \frac{1}{2 \times \nu \times S \times \Delta V}\int I(V)\mathrm{d}V \tag{2}$$

$$C_{\mathrm{A}} = \frac{I \times \Delta t}{\Delta V} \tag{3}$$

where ν is the voltage scan rate (V s^{-1}); S is the total surface area of the device, including the active electrodes and the spacing between electrodes (cm^2), with a value of 0.6728 cm^2 for a single MSC in this work; ΔV is the applied voltage (V); $I(V)$ is the voltammetric current (A); I is the discharge current; and Δt is the discharge time (s).

The volumetric energy density (E_V, Wh cm^{-3}) and power density (P_V, W cm^{-3}) were calculated by equations 4 and 5:

$$E_{\mathrm{V}} = \frac{1}{2} \times \frac{C_{\mathrm{A}}}{d} \times \frac{(\Delta V)^2}{3600} \tag{4}$$

$$P_{\mathrm{V}} = \frac{E_{\mathrm{V}}}{\Delta t} \times 3600 \tag{5}$$

where C_A is the specific areal capacitance (F cm^{-2}) calculated from the charge-discharge curves; d is the thickness of the active material, with a value of ~3×10^{-4} cm for a single MSC in this work; ΔV is the applied voltage (V); and Δt is the discharge time (s).

Results

Fabrication of rGO/Au heterostructured electrodes

rGO/Au heterostructured electrodes were fabricated in three steps: (1) irradiation of a GO film by femtosecond (FS) laser pulses to convert the GO film into rGO interdigitated electrode finger arrays; (2) deposition of a Au metal layer on top of the rGO electrode; and (3) transfer of rGO/Au heterosheets to PDMS (Fig. 1b). Laser-scribed rGO flakes tend to be preferentially oriented perpendicular to the substrate under the specific laser conditions used, which is known as laser texturing[36] or the dynamic growth/etching effect[37]. Here, vertically oriented rGO sheets that were well connected with one another were fabricated by controlling the irradiation conditions of the high-repetition-rate high-power Yb-doped fiber FS laser. The Raman spectra and X-ray diffraction patterns suggested the formation of rGO electrodes with a d-spacing of 3.45 Å (Supplementary Fig. 1a–b). The XPS spectrum

of rGO showed an increased C/O ratio and an intense C-C peak referred to sp2 bonding (Supplementary Fig. 1c–d), which is consistent with the results of Raman and XRD. The rGO had a surface area of ~284 $m^2 g^{-1}$ as measured by BET analysis (Supplementary Fig. 1e), which is comparable to the previous value reported for laser-induced graphene for MSCs[11]. Key parameters for achieving the unique fluff-like morphology of rGO sheets were the fast scan speed (125 mm s^{-1}) and the high-repetition rate (500 kHz) (see Supplementary Fig. 2); the photon energy per pulse was controlled to be lower than the ablation threshold[38], and at the same time, the time interval between FS pulses was short enough, compared to the rate of heat diffusion to the surroundings, to enable conversion of the GO into vertically oriented rGO due to proper heat accumulation[39]. To clarify the effect of the repetition rate, the rGO morphology was tested under different repetition rates, a low repetition rate of 20 kHz and a high-repetition rate of 500 kHz, with the total photon energy per area set to be same (see Supplementary Fig. 3). Severe ablation occurred when the average power at 20 kHz was set the same as that at 500 kHz because the peak power at 20 kHz was 25 times higher than that at 500 kHz; thus, the average power at 20 kHz was set to be 20% of the average power at 500 kHz, and the total exposure energy was compensated by using an 80% slower scan speed instead. Consequently, less vertical (almost 2D structured) rGO was formed at 20 kHz, whereas the high-repetition rate of 500 kHz led to a vertically oriented rGO morphology, which indicated that a high-repetition rate of the FS pulses was beneficial for the vertical rGO arrangement. This vertical morphology allowed a thin gold layer (100 nm Au) to be deposited on the rGO sheets by simple sputtering, forming a vertical heterostructured rGO/Au bilayer network (Supplementary Fig. 4a–d). The unique protruded structure of the rGO/Au sheets allowed the 3D network to be successfully transferred to PDMS without any additional layers or treatments. The vertical Au-coated rGO formed mechanical interlock anchor points that were embedded into the PDMS layer, which would not have been possible simply with planar structures due to the weak physical or chemical interaction between the evaporated Au and PDMS[40]. As a result, the thin Au layer that was embedded between rGO and PDMS made the current collector more stable and lowered the total electronic resistances, while the Au film deposited on the unscribed GO region was easily detached from PDMS due to its highly smooth mirror-like surface and weak interaction with the PDMS[41]. In contrast, the Au-coated rGO with a 2D structure formed by the 20 kHz pulses exhibited unstable features after transfer to PDMS; the rGO/Au film was not embedded into the PDMS, leading to the formation of cracks, even under small deformation (Supplementary Fig. 3).

Conductivity and stretchability of rGO/Au heterosheet electrodes

The rGO/Au/PDMS electrodes had excellent electrical conductivity, as high as 1.3×10^5 S m^{-1}, which was two orders of magnitude better than those of rGO/glass, rGO/PDMS, and previous laser-scribed rGO electrodes[11,13,29] and even comparable to that of flexible rGO–Au NPs on photo paper[33]. The contributions of the additional Au layer were obvious: most of the rGO sheets could be covered and interconnected with a thin Au layer (Supplementary Fig. 5), which enhanced the junction conductance between the rGO sheets. Three samples were prepared with different laser scanning directions with respect to the uniaxial stretching direction, i.e., perpendicular, parallel and both directions with respect to the stretching direction, which are denoted by PD, PL, and BD, respectively, in Fig. 2a. The conductivities of the three samples in various strain states were much higher than that of the vertical rGO embedded in PDMS without a thin Au layer (rGO/PDMS) and close to that of pure Au/PDMS (Fig. 2a). Moreover, even after being stretched to 60%, they still maintained lower levels of sheet resistance than that of rGO/PDMS at 0% strain by factors of 0.67, 0.41, and 0.30 for PD, PL, and BD, respectively (Fig. 2b). Particularly, the BD electrode exhibited even better reversibility than rGO/PDMS, with $\Delta R/R_0$ remaining constant as the strain was released (Fig. 2c). This superior stretchability of the rGO/Au/PDMS is believed to originate from two aspects of the structure. First, the Au layer was adherent and partially embedded between the rGO and PDMS. Generally, as the strain increased, the Au film tended to break or become delaminated out of the plane (Fig. 2d), which led to the generation of large cracks that drastically and abruptly reduced its conductivity. However, in the case of rGO/Au/PDMS, the out-of-plane deformation of the Au layer was suppressed by the conformable rGO and PDMS layers. Moreover, the rGO film was already composed of a network of many rGO flakes of microscale size, inducing high structural stability under stretching (Fig. 2e); thus, the 3D network of rGO/Au could be retained during and after stretching in the same manner (Fig. 2f). Second, the vertically aligned rGO morphology enhanced the stretchability. As evidence, PL and BD exhibited better stretchability than PD because more rGO/Au sheets were connected with each other in the stretching direction in the case of PL and BD, which implies that the rGO morphology could affect the change in conductivity under mechanical deformation. For comparison, we tested two samples: rGO/Au/PDMS electrodes without and with vertically aligned rGO morphology (Fig. 2g and Supplementary Fig. S3), denoted by WOV and WV, respectively. Because the Au layer was deposited in the form of a 2D film, the WOV electrode readily formed large cracks under 50% strain. In fact, the

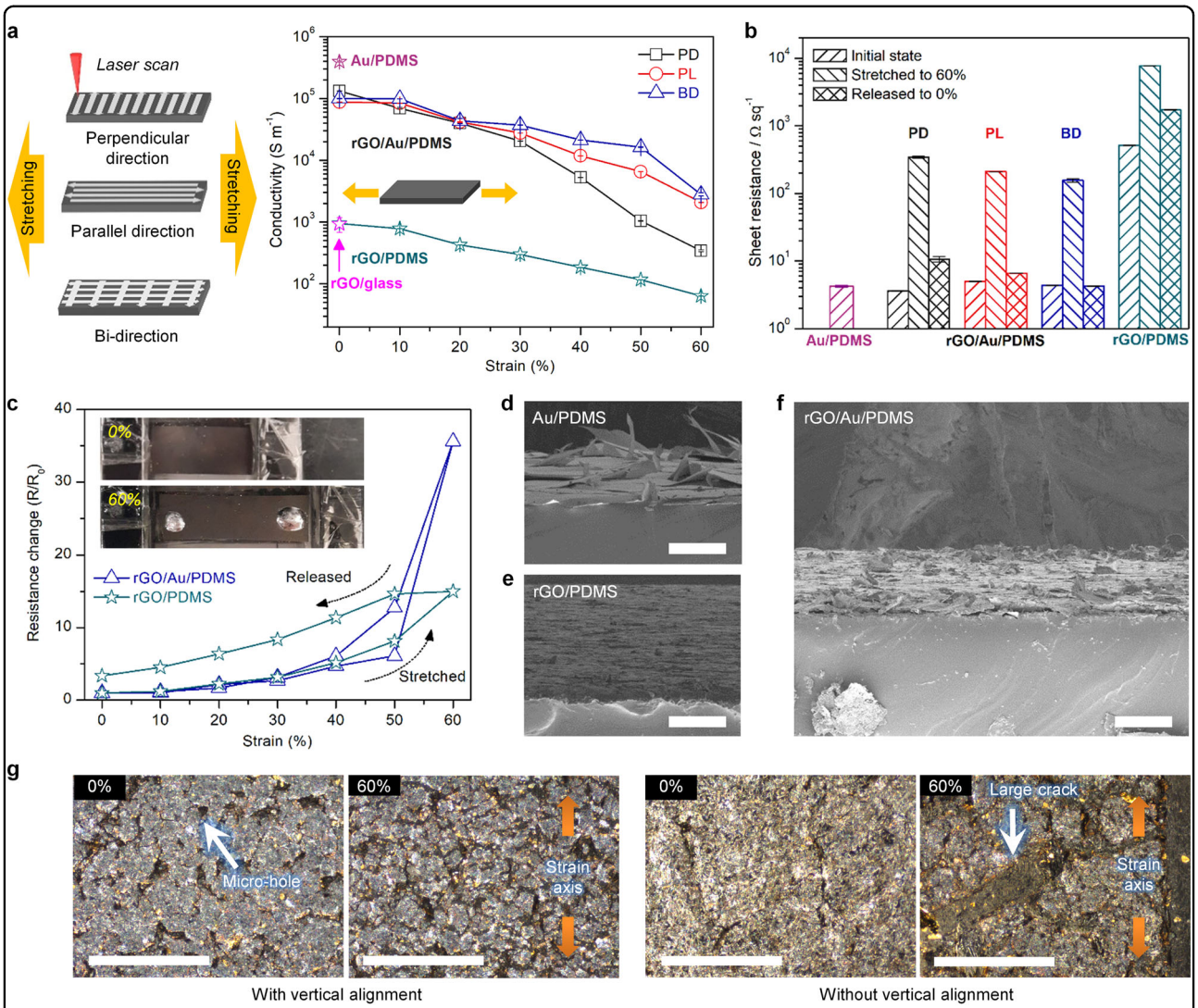

Fig. 2 Conductivity and stretchability of the rGO/Au/PDMS electrodes. a Schematics (from top to bottom) representing electrodes fabricated by FS laser scans in perpendicular (PD), parallel (PL) and both directions (BD) with respect to the stretching axis. The conductivities of the PD, PL, and BD electrodes were measured as a function of tensile strain. Au/PDMS and rGO/PDMS were also compared as control samples. **b** A comparison of the sheet resistance values of Au/PDMS, PD, PL, BD and rGO/PDMS before stretching, under 60% strain and after release to 0% strain. **c** Change in resistance versus tensile strain for BD rGO/Au/PDMS and rGO/PDMS. Both electrodes were stretched to 60% strain and released to 0% strain. The inset shows photographs of a BD electrode under 0% and 60% strain. **d**–**f** Tilted SEM images of **d** Au/PDMS, **e** rGO/PDMS, and **f** rGO/Au/PDMS electrodes after stretching. While the Au film easily broke and torn out of the PDMS, the rGO and rGO/Au electrodes maintained their structures during/after stretching. Scale bar: 20 μm. **g** Microstructural changes of rGO/Au/PDMS electrodes under deformation. The optical images show rGO/Au/PDMS electrodes in which the rGO morphology was tuned with (left) and without (right) vertically oriented structures by controlling the laser condition; each electrode is shown under 0% and 60% strain. Scale bar: 500 μm

WOV electrode started to be torn in two parts at only 5% strain and was easily disconnected after more than 5% strain. The WV electrode, however, exhibited distributed rupture of rGO/Au ligaments because the Au layer was separately deposited on each rGO microsheet from the initial state. Moreover, the rGO/Au flakes standing in vertical directions formed small vacancies in between, as in a nanomesh[42], which suppressed the unexpected generation of large slits and made the contact nodes more stable even under 50% strain. In short, the 3D assembly of rGO/Au heterostructures enabled the formation of electrical contact networks and reduced the contact loss in the stretched state. Therefore, we could attain high conductivity as well as superior intrinsic stretchability in rGO/Au/PDMS; the conductivity was outstanding compared with those of other rGO-based composite

electrodes, including rGO–Ag NPs[34], rGO–poly(vinyl alcohol)[43], rGO–carbon nanotubes–PDMS[44], and rGO–fabric[45], and was even comparable to those of metal NWs/elastomers such as AgNW/PDMS[46] or AgNW/PUA[47].

Electrochemical properties of single MSCs

The rGO/Au heterostructures connected in the 3D network resulted in MSCs with good electrochemical performance and excellent stretchability. MSC electrodes with a neighboring distance of 400 μm were designed and tested under different stretched states in the directions parallel and perpendicular to the microelectrode fingers (Supplementary Fig. 6a, b, respectively). The MSCs exhibited stable CV curves under large strains (0–60%) along both the parallel and perpendicular axes (Fig. 3a and Supplementary Fig. 7a, respectively), verifying their stable electrochemical performance and multiple-axis stretchable properties. Remarkably, due to the reduction of the equivalent series resistance (ESR), the Au layer contributed as a current collector, thereby enhancing the rate capability of the MSCs; e.g., 86% of the capacitance was retained when the scan rate was increased from 0.05 V s^{-1} to 1 V s^{-1}, and 42% was retained for a scan rate increase from 0.05 V s^{-1} to 10 V s^{-1} (Supplementary Fig. 7b). The areal capacitance of the rGO/Au/PDMS at 10 V s^{-1} was superior to those of rGO/glass or rGO/PDMS MSCs; this superiority was preserved even after being stretched to 60% in both the parallel (Fig. 3b) and perpendicular (Supplementary Fig. 7b) directions. The decreased areal capacitance of the rGO/Au/PDMS compared with that of rGO/glass in the region of low scan rates (0.05–0.2 V s^{-1}) implies that some portion of the rGO flakes were embedded in the PDMS elastomer[32]. Interestingly, when subjected to stretching along the parallel axis, the areal capacitance of the rGO/Au/PDMS MSCs in the region of low scan rates (0.05–0.2 V s^{-1}) further increased, which was attributed to the shortened ionic diffusion pathway between two microelectrodes because of the decreased interspacing of the adjacent fingers, promoting electrolyte diffusion and the effective utilization of the electrode material[48]. The areal capacitance of the device under 40% strain along the parallel axis was 0.6 mF cm^{-2} at a scan rate of 0.05 V s^{-1}, which was comparable to those for graphene-based MSCs[12,13,29,31,33,49,50] and prestrained graphene-based stretchable MSCs[26]. EIS analysis also provided consistent insight into the superior performance of rGO/Au/PDMS MSCs even in various stretched states (Fig. 3c and Supplementary Fig. 7c). Nyquist plots of rGO/Au/PDMS revealed a small charge resistance and a lower ESR (18 Ω) than those of rGO/glass (240 Ω) and rGO/PDMS (1.2 kΩ); these ESR values were retained at a low level even after stretching to 60% in the perpendicular and parallel axis directions (denoted by PDA and PLA, respectively). Furthermore, a high characteristic frequency of rGO/Au/PDMS ($f = 22$ Hz, corresponding time constant $\tau = 4.5$ ms) was observed at a −45° phase angle in Bode plots; this frequency was higher than those for rGO/glass (1.26 Hz) and rGO/PDMS (0.4 Hz) and was still preserved at a high level after stretching (Fig. 3d and Supplementary Fig. 7d). Moreover, the rGO/Au/PDMS MSCs showed stable cycling performance; the capacitance was reversibly maintained with 94% retention of the initial value after 20,000 charge-discharge cycles (Fig. 3e). The stable electrochemical performance of the MSCs was further demonstrated by a stretching-releasing test; 95% and 86% of the initial capacitance was maintained after the device was stretched and released under 30% strain for 500 cycles in the perpendicular and parallel directions, respectively (Fig. 3f). This superior performance makes these laser-patterned MSCs promising for stretchable microelectronics.

The performance of this novel platform could be further increased by, for example, exploiting high-capacity materials. As a proof of concept, PANI was electrodeposited on rGO/Au/PDMS electrodes. PANI polymers were deposited on each graphene layer (Supplementary Fig. 8a), the structural stretchability is dependent on the graphene layer morphology even after PANI deposition. In situ optical images of the PANI/rGO/Au/PDMS under various tensile strains (Supplementary Fig. 8b) also confirmed that the change in morphology of the PANI/rGO/Au/PDMS under stretching was similar to that of rGO/Au/PDMS, resulting in distributed rupture of PANI/rGO/Au ligaments under strain. The PANI/rGO/Au/PDMS electrode and MSC presented broad redox peaks (Supplementary Fig. 8c and Fig. 3g), corresponding to the redox transitions of PANI and indicating that the device showed pseudocapacitive behavior[51,52]. The MSC had an areal capacitance of 4.06 m cm^{-2} at 0.2 mA cm^{-2} and retained an areal capacitance of 2.32 mF cm^{-2} at 6 mA cm^{-2} (Fig. 3h), which surpassed previously reported values for stretchable MSCs[22–26]. In addition, the device still exhibited a lower ESR value (82 Ω) than those of rGO/glass and rGO/PDMS (Fig. 3i). Moreover, the device presented good reversible stretchability, with 87% and 84% of the original capacitance being maintained after stretching/releasing at 60% strain in the perpendicular and parallel directions, respectively, and with no substantial changes observed in the CV curves (Fig. 3j). The changes in capacitance in the first stretching/releasing cycle were ascribed to the irreversible sliding and rearrangement of rGO within the elastomer matrix[53]. To further demonstrate the structural durability of MSCs based on PANI/rGO/Au/PDMS, stretching/releasing cycles were conducted (Supplementary Fig. 8d). The capacitance decreased to 85% of its original value in the first 100 cycles and remained constant for an additional

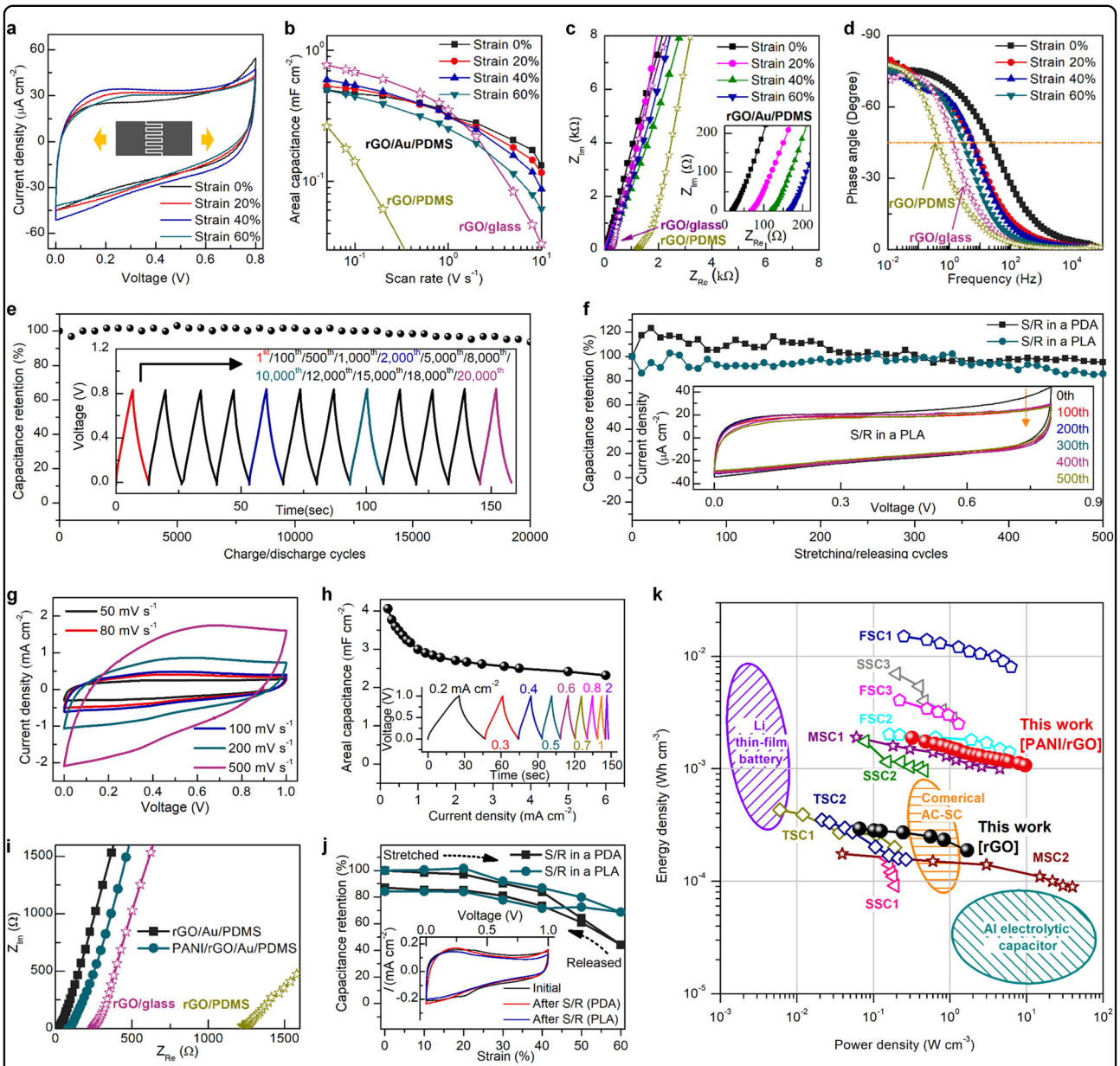

Fig. 3 Electrochemical properties of single MSCs. a–f The electrochemical performance of an MSC based on rGO/Au heterostructures. **a** CV curves at a scan rate of 0.05 V s^{-1}, **b** areal capacitances as a function of scan rate, **c** Nyquist plots (inset shows a magnified high-frequency region), and **d** Bode plots of rGO/Au/PDMS MSCs that were stretched in a direction parallel to the microelectrode fingers, as shown in the schematics (the insets of (**a**)). MSCs of rGO/glass and rGO/PDMS are also compared as control samples. **e** The long-term cycling performance measured at a constant current density of 0.05 mA cm^{-2}. The inset shows highly symmetric charge-discharge profiles and excellent retention over 20,000 consecutive cycles. **f** Specific capacitance retention performance of the device when measurements were conducted after the stipulated number of full stretching/releasing (S/R) cycles in directions perpendicular and parallel to the axis (denoted by PDA and PLA, respectively). The inset shows the CV curves at a scan rate of 0.05 V s^{-1} after every 100 cycles for the device that was stretched/released along the parallel axis. **g–j** The electrochemical performance of the MSC after 30 cycles of polyaniline electrodeposition on rGO/Au/PDMS. **g** CV curves of a single MSC based on polyaniline/rGO/Au/PDMS at different scan rates. **h** Areal capacitance at increasing current densities. The inset shows the galvanostatic charge-discharge curves of the device at increasing current densities. **i** Nyquist plots of polyaniline/rGO/Au/PDMS compared to rGO/glass, rGO/PDMS, and rGO/Au/PDMS. **j** Capacitance retention as a function of tensile strain in directions perpendicular and parallel to the axis (denoted by PDA and PLA, respectively). The samples were reversibly stretched and released back to their original state. The inset shows CV curves of the device before and after being stretched or released (S/R) in PDA and PLA (scan rate: 0.05 V s^{-1}). **k** Ragone plot of single MSCs before and after the electrodeposition of polyaniline as an active material (denoted by rGO and PANI/rGO). The volumetric energy and power density of the devices are compared with those of other stretchable energy storage devices, including sandwich-type supercapacitors (SSC1[52], SSC2[55], and SSC3[59]), fiber-type supercapacitors (FSC1[56], FSC2[51], and FSC3[57]), transparent supercapacitors (TSC1[54] and TSC2[58]), and MSCs (MSC1[23] and MSC2[25])

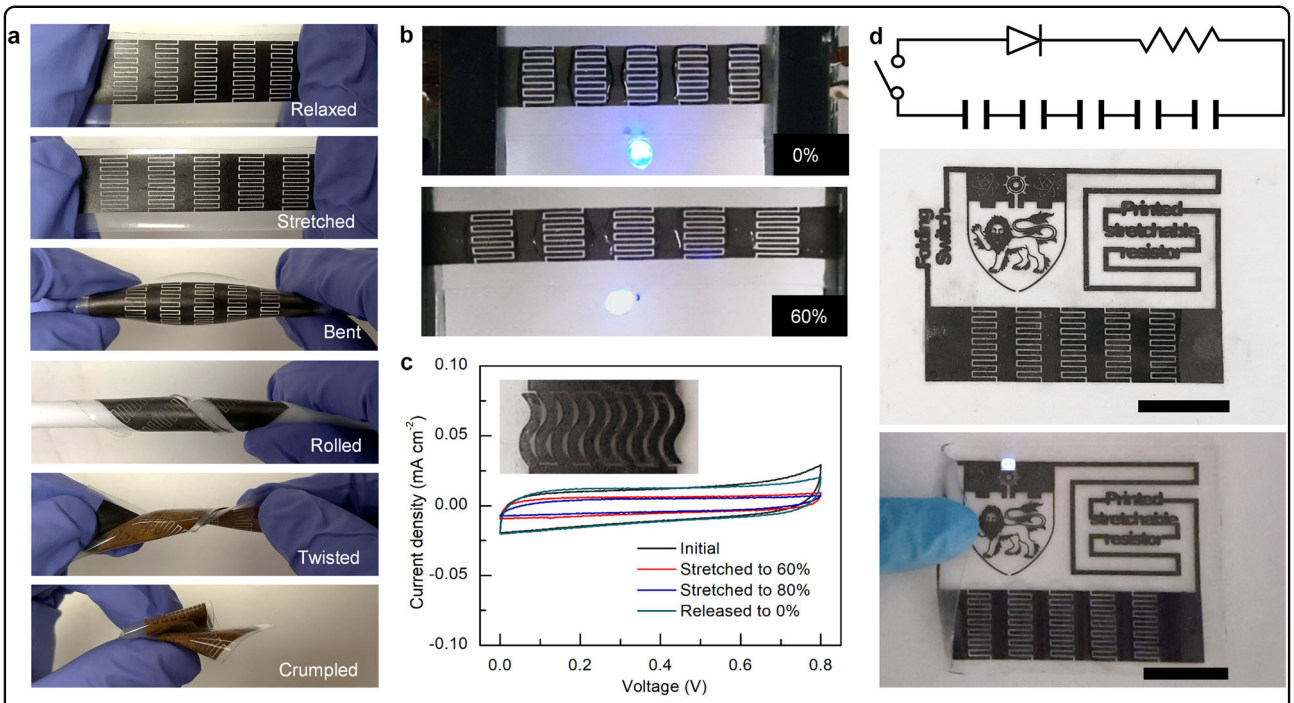

Fig. 4 Demonstrations of laser-patterned elastomeric MSCs with versatile designs. a Photos of five MSCs connected in series (relaxed, stretched, bent, rolled, twisted, and crumpled), showing excellent mechanical robustness. **b** Five series-connected MSCs lit up a commercial LED even under 60% tensile strain, demonstrating an intrinsically stretchable power source. **c** CV curves of a device with a curved pattern that was stretched to 80% and released to 0% in the direction parallel to the microelectrode fingers. The device retained 38% of its original capacitance when stretched to 80% and regained its original value after being released. The inset shows an example of a single MSC with a wavy curved configuration that served to enhance the strain limit to 80%. **d** Schematic equivalent circuit and photographs of the integration of MSCs into a laser-patterned elastomeric circuit based on rGO/Au/PDMS, in which the switch could be turned on/off by folding to create the contact and the resistor could be tuned by the length of the printed circuits and by the stretching-induced change in resistance. Scale bar: 2 cm

400 cycles, demonstrating the mechanical durability and electrochemical stability of the MSCs based on PANI/rGO/Au/PDMS. To evaluate the energy storage properties of the laser-patterned stretchable MSCs, the volumetric energy and power densities were compared with those of various stretchable supercapacitors in a Ragone plot (Fig. 3k). The volumetric energy density (290 μWh cm^{-3}) of the rGO/Au/PDMS supercapacitor was improved compared with those of a carbon-nanotube-based non-intrinsically stretchable MSC[25] and a stretchable sandwich-type supercapacitor[52] and was comparable to those of other graphene-based stretchable supercapacitors[54]. After the electrodeposition of PANI, the device delivered a maximum energy density of 1.88 mWh cm^{-3}, and it still maintained an energy density of 1.07 mW cm^{-3} at a high power density of 9.66 W cm^{-3}; these values are much higher than that of a stretchable MSC with pseudocapacitive capacitance[23] and comparable to those of other types of stretchable supercapacitors[51,55–59].

Demonstrations with versatile laser patterns

One of the most appealing merits of these laser-patterned MSCs is their aesthetic versatility. The laser-patterned MSCs could be readily scaled up: for example, five cells were connected in series without the use of further electric interconnects (Fig. 4a). This device provided a 5-fold increase in voltage (~4 V) compared with a single cell (~0.8 V) and maintained almost 100% capacitance in various mechanically deformed states (Fig. 4a and Supplementary Fig. 9a). It successfully turned on an LED light after sustaining 60% strain, with undistorted charge-discharge behaviors (Fig. 4b and Supplementary Fig. 9b). Furthermore, after charging, the five-MSC array was connected to a wristwatch; the display screen of the watch was lit even under dynamic stretching/releasing at different tensile strains from 15% to 40% (Supplementary Video 1). This behavior demonstrated that our laser-patterning technology allows stretchable MSCs to achieve a stable and tunable output voltage simply through the proper design of the electrode patterns. In addition, the

stretchability of the MSCs could be further enhanced by a wavy curved serpentine electrode of the same size, as shown in Fig. 4c. A single MSC with wavy microelectrode fingers demonstrated stretchability up to 80% tensile strain, with the original capacitance being retained after the MSC was stretched to 80% and released to 0% (Fig. 4c and Supplementary Fig. 10). Moreover, as a proof of concept for practical applications, with a particular focus on wearable electronics or IoT devices, the MSCs and electrical circuits were assembled in digital images with various form factors through laser patterning. As illustrated in Fig. 1, a freeway-like MSC with five cells connected in series was laser patterned and esthetically unified with a letter-shaped electric circuit. This unobstrusive and elastomeric power source could be attached to any curved/irregular surface or appliance or could be worn on a human body and could be used to successfully power a watch or LED even under deformation (Fig. 1 and Supplementary Video 2). To further highlight the unique functions of these laser-patterned MSCs as integrated power sources for fully independent elastomeric electronics, we fabricated an MSC-inclusive elastic circuit composed of a letter-shaped folding switch, a stretching-induced variable resistor, and an LED-embedded Nanyang Technological University (NTU) logo, as shown in Fig. 4d. After charging, the LED light bulb connected to the logo circuit was lit up (Fig. 4d), and the LED could be turned on and off more than ten times by folding and releasing the switch, respectively (Supplementary Video 3), demonstrating the use of the MSCs for autonomous elastomeric electronics. These results confirmed the wide range of applications of the laser-patterned MSCs as monolithically embedded power sources in diverse future soft electronic systems.

Discussion

In conclusion, we have shown that high-performance elastomeric MSCs can be fabricated using a facile and versatile direct-laser-patterning method without employing geometric engineering or stretchable interconnects. This was accomplished via a highly conductive and stretchable rGO/Au heterostructure, in which femtosecond-laser-induced, vertically oriented graphene flakes accommodate a large strain and their electrical connections are reinforced by the connected Au layer. The fabrication process is simple and straightforward: planar MSCs with interdigital electrode fingers are patterned by laser scanning, followed by the deposition of Au and transfer to PDMS. The resulting MSCs exhibit rubbery elasticity in every direction, can be operated at large strains (up to 60%), and show a significantly improved rate capability and frequency response in the stretched state. The energy density can be further increased by incorporating higher-capacity electrode materials. Notably, the fabrication process is scalable and can be readily adapted to versatile designs, allowing MSCs to be patterned with other elastomeric devices. These stretchable MSCs can be easily connected in series, enabling the user-customized tuning of the cell voltage. The stretchability of the MSCs can also be controlled by designing the electrodes in wavy/curved shapes. As a final step, we demonstrated that these MSCs can be aesthetically unified with other laser-patterned elastomeric circuits and electronics, featuring computer-designed artistic patterns and letters. Such intrinsically stretchable integrated power sources will facilitate the wider use of elastomeric electronics in wearable electronics, soft robotics, and the Internet of Things.

Acknowledgements

This work was supported by the NRF Investigatorship, Award No. NRF-NRFI2016-05. This work was also financially supported by an NRF Fellowship (NRF-NRFF2015-02) from the Singapore National Research Foundation and an AcRF Tier 1 grant (RG180/16) from the Singapore Ministry of Education.

Author Contributions

S.P., H.L., Y.-J.K. and P.S.L. conceived of the concept, processing and structural details. S.P. and H.L. performed the material fabrication and tests, conducted the data analyses and wrote the manuscript. Y.-J.K. and P.S.L. directed the experiments and contributed to the writing of the manuscript. All authors discussed the results and commented on the manuscript.

Conflict of Interest

The authors declare no conflict of interest.

Supplementary information is available for this paper at https://doi.org/10.1038/s41427-018-0080-z.

Received: 2 March 2018 Revised: 28 April 2018 Accepted: 14 June 2018.
Published online: 3 October 2018

References

1. Rogers, J. A., Someya, T. & Huang, Y. Materials and mechanics for stretchable electronics. *Science* **327**, 1603–1607 (2010).
2. McCoul, D., Hu, W., Gao, M., Mehta, V. & Pei, Q. Recent advances in stretchable and transparent electronic materials. *Adv. Electron. Mater.* **2**, 1500407 (2016).
3. Trung, T. Q. & Lee, N. E. Recent progress on stretchable electronic devices with intrinsically stretchable components. *Adv. Mater.* **29**, 1603167 (2017).
4. Yan, C. & Lee, P. S. Stretchable energy storage and conversion devices. *Small* **10**, 3443–3460 (2014).
5. Liu, W., Song, M. S., Kong, B. & Cui, Y. Flexible and stretchable energy storage: recent advances and future perspectives. *Adv. Mater.* **29**, 1603436 (2017).
6. Kyerematen, N. A., Brousse, T. & Pech, D. Microsupercapacitors as miniaturized energy-storage components for on-chip electronics. *Nat. Nanotechnol.* **12**, 7–15 (2017).
7. Qi, D., Liu, Y., Liu, Z., Zhang, L. & Chen, X. Design of architectures and materials in in-plane micro-supercapacitors: current status and future challenges. *Adv. Mater.* **29**, 1602802 (2017).
8. Tyagi, A., Tripathi, K. M. & Gupta, R. K. Recent progress in micro-scale energy storage devices and future aspects. *J. Mater. Chem. A* **3**, 22507–22541 (2015).
9. Zhang, Y. Z. et al. Flexible supercapacitors based on paper substrates: a new paradigm for low-cost energy storage. *Chem. Soc. Rev.* **44**, 5181–5199 (2015).

10. Choi, K.-H., Yoo, J., Lee, C. K. & Lee, S.-Y. All-inkjet-printed, solid-state flexible supercapacitors on paper. *Energy Environ. Sci.* **9**, 2812–2821 (2016).
11. Lin, J. et al. Laser-induced porous graphene films from commercial polymers. *Nat. Commun.* **5**, 5714 (2014).
12. Gao, W. et al. Direct laser writing of micro-supercapacitors on hydrated graphite oxide films. *Nat. Nanotechnol.* **6**, 496–500 (2011).
13. El-Kady, M. F. & Kaner, R. B. Scalable fabrication of high-power graphene micro-supercapacitors for flexible and on-chip energy storage. *Nat. Commun.* **4**, 1475 (2013).
14. Li, L. et al. High-Performance Solid-State Supercapacitors and Micro-supercapacitors Derived from Printable Graphene Inks. *Adv. Energy Mater.*, **6**, 1600909 (2016).
15. Liu, W. et al. Paper-based all-solid-state flexible micro-supercapacitors with ultra-high rate and rapid frequency response capabilities. *J. Mater. Chem. A* **4**, 3754–3764 (2016).
16. Jung, H., Ve Cheah, C., Jeong, N. & Lee, J. Direct printing and reduction of graphite oxide for flexible supercapacitors. *Appl. Phys. Lett.* **105**, 053902 (2014).
17. Liu, S. et al. Nitrogen-doped reduced graphene oxide for high-performance flexible all-solid-state micro-supercapacitors. *J. Mater. Chem. A* **2**, 18125–18131 (2014).
18. Savagatrup, S., Printz, A. D., O'Connor, T. F., Zaretski, A. V. & Lipomi, D. J. Molecularly stretchable electronics. *Chem. Mater.* **26**, 3028–3041 (2014).
19. Park, S., Parida, K. & Lee, P. S. Deformable and transparent ionic and electronic conductors for soft energy devices. *Adv. Energy Mater.* **7**, 1701369 (2017).
20. Oh, J. Y. et al. Intrinsically stretchable and healable semiconducting polymer for organic transistors. *Nature* **539**, 411–415 (2016).
21. Kumar, R. et al. All-printed, stretchable Zn-Ag2O rechargeable battery via hyperelastic binder for self-powering wearable electronics. *Adv. Energy Mater.* **7**, 1602096 (2017).
22. Kim, D., Shin, G., Kang, Y. J., Kim, W. & Ha, J. S. Fabrication of a stretchable solid-state micro-supercapacitor array. *ACS Nano* **7**, 7975–7982 (2013).
23. Lee, G. et al. Fabrication of a stretchable and patchable array of high performance micro-supercapacitors using a non-aqueous solvent based gel electrolyte. *Energy Environ. Sci.* **8**, 1764–1774 (2015).
24. Kim, H. et al. Encapsulated, high-performance, stretchable array of stacked planar micro-supercapacitors as waterproof wearable energy storage devices. *ACS Appl. Mater. Interfaces* **8**, 16016–16025 (2016).
25. Pu, J., Wang, X., Xu, R. & Komvopoulos, K. Highly stretchable micro-supercapacitor arrays with honeycomb structures for integrated wearable electronic systems. *ACS Nano* **10**, 9306–9315 (2016).
26. Qi, D. et al. Suspended wavy graphene microribbons for highly stretchable microsupercapacitors. *Adv. Mater.* **27**, 5559–5566 (2015).
27. Li, L. et al. Highly stretchable micro-supercapacitor arrays with hybrid MWCNT/PANI electrodes. *Adv. Mater. Technol.* **2**, 1600282 (2017).
28. Xie, K. & Wei, B. Materials and structures for stretchable energy storage and conversion devices. *Adv. Mater.* **26**, 3592–3617 (2014).
29. El-Kady, M. F., Strong, V., Dubin, S. & Kaner, R. B. Laser scribing of high-performance and flexible graphene-based electrochemical capacitors. *Science* **335**, 1326–1330 (2012).
30. Beidaghi, M. & Wang, C. Micro-supercapacitors based on interdigital electrodes of reduced graphene oxide and carbon nanotube composites with ultrahigh power handling performance. *Adv. Func. Mater.* **22**, 4501–4510 (2012).
31. Wu, Z. S., Parvez, K., Feng, X. & Mullen, K. Graphene-based in-plane micro-supercapacitors with high power and energy densities. *Nat. Commun.* **4**, 2487 (2013).
32. Lamberti, A., Clerici, F., Fontana, M. & Scaltrito, L. A highly stretchable supercapacitor using laser-induced graphene electrodes onto elastomeric substrate. *Adv. Energy Mater.* **6**, 1600050 (2016).
33. Li, R. Z. et al. High-rate in-plane micro-supercapacitors scribed onto photo paper using in situ femtolaser-reduced graphene oxide/Au nanoparticle microelectrodes. *Energy Environ. Sci.* **9**, 1458–1467 (2016).
34. Yoon, Y. et al. Highly stretchable and conductive silver nanoparticle embedded graphene flake electrode prepared by in situ dual reduction reaction. *Sci. Rep.* **5**, 14177 (2015).
35. Li, S. et al. A high-performance lithium-ion capacitor based on 2D nanosheet materials. *Small* **13**, 1602893 (2017).
36. Viskadouros, G., Konios, D., Kymakis, E. & Stratakis, E. Direct laser writing of flexible graphene field emitters. *Appl. Phys. Lett.* **105**, 203104 (2014).
37. Deng, N.-Q. et al. Tunable graphene oxide reduction and graphene patterning at room temperature on arbitrary substrates. *Carbon* **109**, 173–181 (2016).
38. Kerse, C. et al. Ablation-cooled material removal with ultrafast bursts of pulses. *Nature* **537**, 84–88 (2016).
39. Gattass, R. R. & Mazur, E. Femtosecond laser micromachining in transparent materials. *Nat. Photonics* **2**, 219–225 (2008).
40. Loo, Y.-L., Willett, R. L., Baldwin, K. W. & Rogers, J. A. Additive, nanoscale patterning of metal films with a stamp and a surface chemistry mediated transfer process: applications in plastic electronics. *Appl. Phys. Lett.* **81**, 562–564 (2002).
41. Byun, I., Coleman, A. W. & Kim, B. Transfer of thin Au films to poly-dimethylsiloxane (PDMS) with reliable bonding using (3-mercaptopropyl)tri-methoxysilane (MPTMS) as a molecular adhesive. *J. Micromech. Microeng.* **23**, 085016 (2013).
42. Guo, C. F., Sun, T., Liu, Q., Suo, Z. & Ren, Z. Highly stretchable and transparent nanomesh electrodes made by grain boundary lithography. *Nat. Commun.* **5**, 3121 (2014).
43. Hou, C. et al. A strong and stretchable self-healing film with self-activated pressure sensitivity for potential artificial skin applications. *Sci. Rep.* **3**, 3138 (2013).
44. Chen, M. et al. Highly stretchable conductors integrated with a conductive carbon nanotube/graphene network and 3D porous Poly(dimethylsiloxane). *Adv. Func. Mater.* **24**, 7548–7556 (2014).
45. Zhao, C., Shu, K., Wang, C., Gambhir, S. & Wallace, G. G. Reduced graphene oxide and polypyrrole/reduced graphene oxide composite coated stretchable fabric electrodes for supercapacitor application. *Electrochim. Acta* **172**, 12–19 (2015).
46. Yao, S. & Zhu, Y. Nanomaterial-enabled stretchable conductors: strategies, materials and devices. *Adv. Mater.* **27**, 1480–1511 (2015).
47. Liang, J., Li, L., Niu, X., Yu, Z. & Pei, Q. Elastomeric polymer light-emitting devices and displays. *Nat. Photonics* **7**, 817–824 (2013).
48. Liu, W., Lu, C., Wang, X., Tay, R. Y. & Tay, B. K. High-performance micro-supercapacitors based on two-dimensional graphene/manganese dioxide/silver nanowire ternary hybrid film. *ACS nano* **9**, 1528–1542 (2015).
49. Yoo, J. J. et al. Ultrathin planar graphene supercapacitors. *Nano Lett.* **11**, 1423–1427 (2011).
50. Wu, Z.-S., Parvez, K., Feng, X. & Müllen, K. Photolithographic fabrication of high-performance all-solid-state graphene-based planar micro-supercapacitors with different interdigital fingers. *J. Mater. Chem. A* **2**, 8288 (2014).
51. Jin, H. et al. High-performance fiber-shaped supercapacitors using carbon fiber thread (CFT)@polyanilne and functionalized CFT electrodes for wearable/stretchable electronics. *Nano Energy* **11**, 662–670 (2015).
52. Yu, M. et al. Water surface assisted synthesis of large-scale carbon nanotube film for high-performance and stretchable supercapacitors. *Adv. Mater.* **26**, 4724–4729 (2014).
53. Yan, C. et al. Stretchable Silver-Zinc batteries based on embedded nanowire elastic conductors. *Adv. Energy Mater.* **4**, 1301396 (2014).
54. Li, N. et al. Free-standing and transparent graphene membrane of polyhedron box-shaped basic building units directly grown using a NaCl template for flexible transparent and stretchable solid-state supercapacitors. *Nano Lett.* **15**, 3195–3203 (2015).
55. Lv, T., Yao, Y., Li, N. & Chen, T. Highly stretchable supercapacitors based on aligned carbon nanotube/molybdenum disulfide composites. *Angew. Chem. Int. Ed. Engl.* **55**, 9191–9195 (2016).
56. Li, M., Zu, M., Yu, J., Cheng, H. & Li, Q. Stretchable fiber supercapacitors with high volumetric performance based on buckled MnO2 /oxidized carbon nanotube fiber electrodes. *Small* **13**, 1602994 (2017).
57. Shi, M. et al. Stretchable wire-shaped supercapacitors with high energy density for size-adjustable wearable electronics. *Chem. Eng. J.* **322**, 538–545 (2017).
58. Park, S., Tan, A. W. M., Wang, J. & Lee, P. S. Coaxial Ag–base metal nanowire networks with high electrochemical stability for transparent and stretchable asymmetric supercapacitors. *Nanoscale Horiz.* **2**, 199–204 (2017).
59. Kim, B. S. et al. 2D reentrant auxetic structures of graphene/CNT networks for omnidirectionally stretchable supercapacitors. *Nanoscale* **9**, 13272–13280 (2017).